From 3D grassy vegetation point cloud to hydraulic resistance: Application to close-range estimation of Manning coefficients for intermittent open channels

F. Vinatier, Jean-Stéphane Bailly, Gilles Belaud

From 3*D* grassy vegetation point cloud to hydraulic resistance: Application to close-range estimation of Manning coefficients for intermittent open channels

F. Vinatier[a,*], J.-S. Bailly[b], G. Belaud[c]

[a] *INRA, UMR LISAH, F-34060 Montpellier, France*
[b] *AgroParisTech, UMR LISAH, F-34060 Montpellier, France*
[c] *SupAgro, UMR GEAU, F-34093 Montpellier, France*

Abstract

The understanding of interrelations between biotic and abiotic processes in intermittent open-channels is currently of primary importance to better assess the services and disservices they provide. A large body of literature attempts to characterize vegetation functional traits affecting hydraulic rugosity, through the introduction of the blockage factor of flow by vegetation. However, this factor has multiple definitions and is still difficult to assess in the fields with actual and diverse vegetation covers, especially for grassy plants of ditches. Our study aims at predicting flow resistance from 3*D* vegetation characteristics using a close-range laser scanner. Flow resistance and vegetation 3*D* characteristics were defined using Manning coefficient and blockage factors, respectively. We tested combined effects of flow discharge against plant species and densities characterizing intermittent channels in a channel flume. Our results showed a variability of Manning coefficient describing flow rugosity against species and densities, with a highest rugosity for sclerophyllous species than herbaceous ones. Different blockage factors were calculated on the basis of scan clouds linked to Manning coefficients using non linear equation. The best relationship (R^2 = 0.9) were found for non linear equation relating Manning coefficients to a simplified blockage factor figuring the mean vegetation height deduced from the projection of the scan point cloud to the channel frontal area. The introduction of a coefficient to correct underestimated values issued from herbaceous species considering their reconfiguration under hydrodynamic loading is thus discussed.

Keywords: plant architecture, Terrestrial Lidar Scanner, 3D, hydraulics, ditch,

Highlights

- We built a hydraulic experimental setup composed of real plants frequently found in Mediterranean ditches in a channel flume to analyze the effect of vegetation diversity and density on hydraulic resistance.
- We used a scanner laser to measure vegetation point clouds and estimate several blockage factor induced by vegetation cover.
- The blockage factor explained 90% of flow resistance deduced from the total head loss at the channel scale.
- The results we found allow the objective pre-determination of resistance factors for intermittent grassy open-channels (irrigation channels, drainage ditches) using close-range vegetation size estimation technics.

1. Introduction

Intermittent open-channels in cultivated landscapes consist of irrigation channels, road-side ditches, drainage ditches and reshaped gullies that have been built for centuries (Lepart & Debussche, 1992) to convey water to plots or conversely, to catch the excess of water from plots or roads and convey them to rivers. They are mainly made of soft soil material where vegetation can grow, requiring channel vegetation management (Levavasseur et al., 2014).

As a consequence, the vegetation of intermittent open-channels and its dynamics could provide numerous ecosystem disservices and services (Dollinger et al., 2015) by affecting the former channel hydraulic conveyance capacities, by trapping and tranporting sediments, nutrients and pollutants, making them biogeochemicals hotspots in addition to be ecological hotspots (Herzon & Helenius, 2008).

In turn, intensities of these services and disservices result from complex interrelations between biotic and abiotic processes (Wiens, 2002; Thomas et al., 2014), governed by channel hydraulics (flow height, residence time, flow velocity field) depending on plant functional traits (Kouwen et al., 1969) such as the drag at the blade or plant scale, or integrated resistance factors at the patch or reach scales. The study of plant functional traits of interest (e.g. plant size and architecture), are usually carried out by agro-ecological insights (Colbach et al., 2014) but it also appears of primary importance to conduct researches at the interface between ecology and hydrology in order to study the diversity of plant functional traits against water flows (Nikora, 2010).

The link between vegetation and flow chacteristics is the

*Corresponding author
Email address: fabrice.vinatier@supagro.inra.fr (F. Vinatier)

subject of many studies in eco-hydraulics reviewed by Curran & Hession (2013); Nepf (2012); Vargas-Luna et al. (2015). In particular, it was shown that vegetated channel flows could be approached with Nikuradse (1933)'s model, making the link between local shear stress and velocity distribution (Stephan & Gutknecht, 2002).

Many studies can be found in the literature, linking vegetation characteristics to local flow properties (Järvelä, 2005; Luhar & Nepf, 2013). Vargas-Luna et al. (2015) analyzed performances of hydraulic models on 13 and 27 experimental studies linking flow resistance to real and artificial vegetation, respectively. Vegetation effects on flows were deduced from the rigid-cylinder analogy that considered a characteristic diameter, average height and distance between plant similar for each experiment.

Applying these concepts to real systems raises major issues, such as the characterisation of vegetation properties, the effect of vegetation heterogeneity, or the upscaling from plant scale to reach scale (Folkard, 2011).

Advances have been done at plant scale by Weissteiner et al. (2015) and Jalonen & Järvelä (2014), thanks to an original setup implying a towing tank and fully digitized riparian trees, they explored the plant reconfiguration under hydrodynamic loading. Cassan et al. (2015) could show the good correspondence between local shear stress and reach scale resistance, but vegetation properties could be estimated only indirectly through their effect on flow characteristics. Flows with emergent vegetation typical of intermittent channels were much less investigated, notably because of the difficulty to explore velocity fields within the vegetation (Pasquino et al., 2016), despite some advances in this field using numerical experiments (Boothroyd et al., 2016).

Green (2005b) summarized the main concepts to calculate the resistance in the light of the nature and size of vegetation, and obtained a non-linear relationship between channel resistance and the proportion of the channel occupied by vegetation, suggesting its first order effect on flow resistance.

However, the vegetation resistance cannot be observed directly: it is empirically calibrated and rarely defined at the reach scale. Green (2005a) identified the vegetation size parameters, usually resumed in a "blockage factor" included in different formulations of roughness estimation due to vegetation (Fisher, 1992). Blockage factor covers different vegetation size metrics and scales. It initially denoted at a given abscissae of the reach, the cross-sectional blockage factor consisting of the proportion of the wetted cross-section occupied by plant stands (Watson, 1987; Jalonen et al., 2014). When sampled regularly along the reach, it corresponds at reach scale to the average ponctual cross-sectional blockage factors (Champion & Tanner, 2000).

It results now multiple definitions of vegetation size metrics linked to resistance parameters at reach scale with different levels of difficulties to estimate it. This latter point lead Green (2005b) to conclude that surface area blockage factor had to be preferred, since measuring the vegetation size, especially at patch, stand or reach scale is a difficult task that depends on vegetation complexity. Recently, a large amount of litterature attempted to approach the blockage factor using direct measures in the fields and in the laboratory, depending on plant type. The Leaf Area Index (LAI) or the leaf to stem area ratio was introduced as a vegetation density measure of the blockage factor (Jalonen et al., 2012; Jalonen & Järvelä, 2014) for woody vegetation. Jalonen et al. (2015) characterized the mixed floodplain vegetation in order to derive metrics for hydraulic analyses. They found that mean heights of vegetation were best related to their frontal areas for herbaceous vegetation whereas a complete view of their 3D structure was necessary for woody plants.

The recent spread of Terrestrial Laser Scanner (TLS) offers possible vegetation size estimations from in-field experiments for hydraulic applications (Jalonen et al., 2012, 2015; Boothroyd et al., 2016). The TLS helped characterizing the height distribution and the volumetric blockage factor of plant communities at channel scale (Jalonen et al., 2014, 2015), or the complete morphology of single trees (Boothroyd et al., 2016).

To our knowledge, although the empirical evidence of considering vegetation properties to infer flow transport (Vargas-Luna et al., 2015), and the potential of using TLS for pre-determination of reach roughness parameters (Jalonen et al., 2015), there is no empirical study linking vegetation point clouds derived from TLS scans to open-channel roughness coefficients, and especially for grassy plants that can be found in intermittent open channels of cultivated landscapes. Grassy plants have a small size and a large range of morphological variability and flexibiliy among species (Kattge et al., 2011), ranging from the herbaceous ones, very flexible, to the sclerophyllous plants that had hard leaves and/or stems.

This paper aims at investigating how different channel vegetation size metrics estimated from scanner laser point clouds may lead to the estimation of Manning roughness coefficient resulting from total head loss during steady flow. The study is based on original experiments using actual grassy plant material, both herbaceous and sclerophyllous, installed in a flume with controlled hydraulic conditions. The main originality of the paper comes from the attempt to link real grassy vegetation clouds to Manning roughness coefficients.

We first expose the factorial experimental setup regarding flow discharge, plant species and plant densities implemented on the channel bed. The different vegetation size metrics at the reach scale from scanner-laser data are then exposed. We finally test the statistical modelling between vegetation metrics and Manning coefficients. Results are then discussed in comparison to those obtained by Green (2005b) and (Jalonen et al., 2015; Jalonen & Järvelä, 2014).

2. Material and methods

2.1. The experimental flume

Experiments were conducted in a channel with cement borders of length 13 m, width 0.67 m, and depth 0.40 m, located in the hydraulic laboratory of Montpellier, Supagro (43.62N, 3.85W) (Figure 2). The channel was chosen according to its dimensions similar in terms of geometry and Froude number to agricultural ditches of the Languedoc vineyards area, avoiding scale effects. The downstream water level was imposed by

a rectangular weir. Flow turbulencies were minimized using a flow tranquilizer located upstream (Figure 1). The channel bottom was covered with high-density polystyrene plates pierced at a density of 328 $holes.m^{-2}$ arranged on a regular grid. Holes were filled with plastic dowels to facilitate plants push down and manipulation.

The channel slope S_b was 1.3/1000. The discharge was maintained constant thanks to level control structures and baffle sluice gates located upstream of the flume. Discharges were checked by velocity integration on the wetted area (10 verticals, 5 points per vertical). Local velocities were explored using a current meter (Hydreka©M801). The two selected flow rates were 25.3 to 51.4 $L.s^{-1}$, with an accuracy of 5%.

Water depth was measured using point gauges installed at the upstream end, the middle and the downstream end of the flume. Since uniform flow is hardly achievable in such conditions, roughness was obtained from the headloss in the channel. Therefore, the accuracy of the measured differences between upstream and downstream levels was crucial. This accuracy is affected by the fixed error between the gauges (incertainty estimated lower than 0.5mm, thanks to precision levelling with still water), and by the reading of levels during experiments. The effect of water fluctuations was analyzed by different means: pressure level sensors (Keller 46X/0.1Bar, accuracy 0.01% of full scale in the range of the experiments) and digital cameras. The analysis showed that most incertainties were due to water fluctuations (±1mm) observed at the free surface. Since flows are clearly subcritical, these fluctuations were rather limited, but they induced an incertainty between 1 and 2mm on the measured headloss. The lowest incertainties could be achieved by increasing the number of readings, which was essential for configurations with the lowest headloss (around 5mm between most distant gauges). Water depths ranged from 18.9 to 26.7 cm over all experiments. Mean velocities ranged between 0.26 and 0.38 $m.s^{-1}$. Manning roughness coefficient of the empty channel was estimated by removing all plants. A value of $0.02 \pm 0.005 s.m^{1/3}$ was obtained for both reference discharges.

Six targets were fixed on channel curbstones to align TLS scans. Position of targets and gauges were precisely located using a tacheometer at a 0.5 mm accuracy.

2.2. Plant material

Four plant species were selected according to their hydrophilic behaviour on a gradient from xerophylous (*Asparagus acutifolius*) to hydrophylous (*Lythrum salicaria*) wich is in accordance with their upstream-dowstream location in the drainage network, branching complexity and their abundance in ditches of the Southern France landscapes (Marnotte & Carrara, 2006): *Asparagus acutifolius*, *Lythrum salicaria*, *Elytrigia repens*, and *Scirpoides holoschoenus*, these last two species being considered as herbaceous, while the two others can be considered as sclerophyllous (Figure 3). In order to get correct estimates of plant densities in real ditches, a sampling campaign was conducted in the Languedoc area (43.478N, 3.338W) in March 2013 to estimate the vegetation densities for all species in similar channels by counting total plant number per 0.48 m^2 quadrat in eight sites, leading to a density of $170 \pm 100 plants.m^{-2}$ (Benitou, 2013).

Approximately 1600 plants of each species were collected in the Languedoc area just before experiments to prevent dessication and keep the initial roughness properties of plant material. Then each plant was cut at the basis to get calibrated 40 ±5 cm length replicates, i.e. above the water depths of the setup, leading to a determination of flow resistance in case of non-submerged vegetation (Järvelä, 2004).

According to Jalonen & Järvelä (2014); Weissteiner et al. (2015), properties of plants are described in terms of projected areas, architecture and leaf to stem area ratios. Ten random samples of each plant were photographed laterally against white background in still air, and then area and stem parts were digitized from the scaled pictures to determine vegetation properties (Table 1). We conserved ramification variabilities occuring in the field. Only herbaceous plants were sometimes ramified, with a maximal axis order between 1 and 3 for *Lythrum salicaria* and between 2 and 3 for *Asparagus acutifolius* (axis order is determined according to rules of the Multi-scale Tree Graph formalism (Godin & Caraglio, 1998). Each *Elytrigia repens* sampled consisted in one main shoot and one or two tillers, figuring herbaceous tillering. Each *Scirpoides holoschoenus* sample consisted in only one main shoot.

2.3. Tested vegetation densities

Five increasing vegetation densities were settled at the channel bottom, with various plant densities for a regular pattern along channel width and staggered along channel length, varying respectively from 0 to 41, 82, 164 and 328 $plants.m^{-2}$. The corresponding nearest distances between plants varied from 14, 10, 7, and 5 cm, respectively, in line with the variabilities observed in the field.

2.4. Estimation of plant reconfiguration in flow

According to Weissteiner et al. (2015), plant reconfiguration could be estimated by the underwater frontal projected area (FPA), giving deflected height and contracted width of the plant. Mounting cameras underwater at a distance preventing hydraulic artefacts and allowing plants observations under small water depths was not possible in our setup with small water depths. However, two cameras disposed on channel upstream and downstream borders and a third camera was located at nadir 6 meters above the channel with vertical recording position (cameras and gauge positions were illustrated in Figure 1). This allowed us to observe qualitatively if plant reconfiguration occurs during flow.

2.5. Data clouds measure

Data clouds were measured in absence of flow using a 1064 nm terrestrial lidar scanner (TLS) branded RIEGL©VZ400 located at nadir 5 meters above the channel with vertical scan position at mid length to prevent too high incident angles. The RIEGL©VZ400 a spot size of 4 mm, a scan rate up to 700,000 points/s, and a range up to 200 m. The selected field of view for the experiment was 80° × 160° and the horizontal and vertical

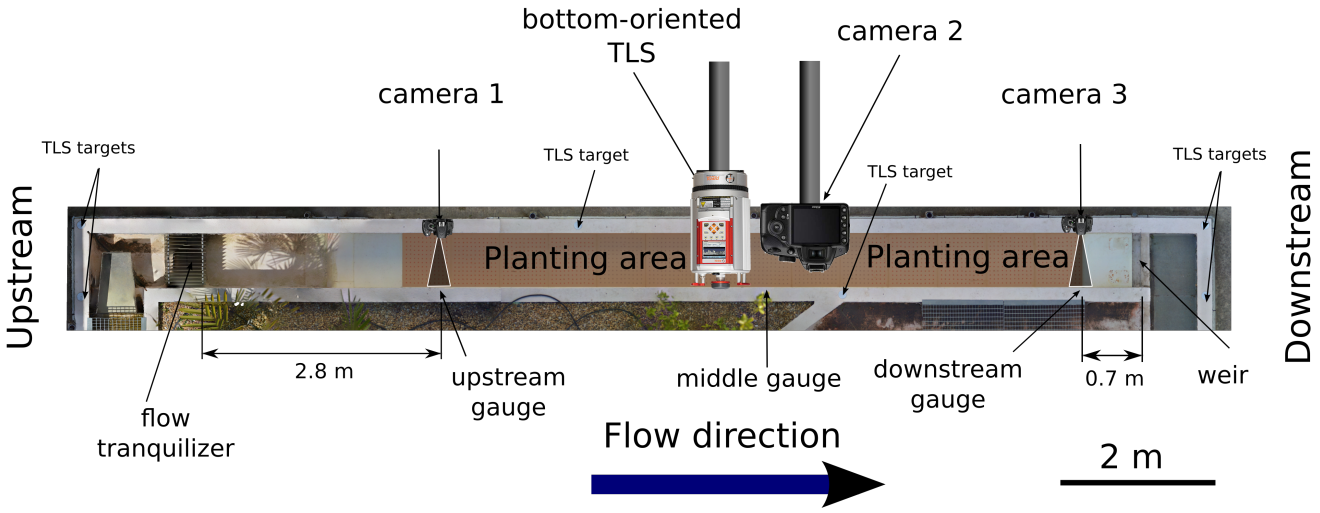

Figure 1: Vertical view of the experimental setup.

Plant species	Basal stem diameter (cm)	Plant height (cm)	Plant width (cm)	Frontal projected area (FPA) (cm^2)	Leaf to steam area ratio
Asparagus acutifolius	0.28 (0.16-0.36)	41.5 (29-48)	25.2 (9-47)	172.1 (86-248)	2.45 (2.2-2.7)
Elytrigia repens	1.01 (0.9-1.2)	45.5 (35-57)	24.2 (16-35)	81.0 (50-157)	-
Lythrum salicaria	0.63 (0.4-0.8)	42.1 (37-45)	16.0 (8-20)	185.7 (26-366)	0.62 (0.2-1.1)
Scirpoides holoschoenus	0.47 (0.43-0.54)	40.6 (38-45)	5.7 (3-11)	19.4 (16-25)	-

Table 1: Table representing the mean geometric characteristics of the plant species over ten samples. Values in brackets correspond to the min-max. Note that the leaf to stem area ratio was not calculated for herbaceous species (indicated by a -)

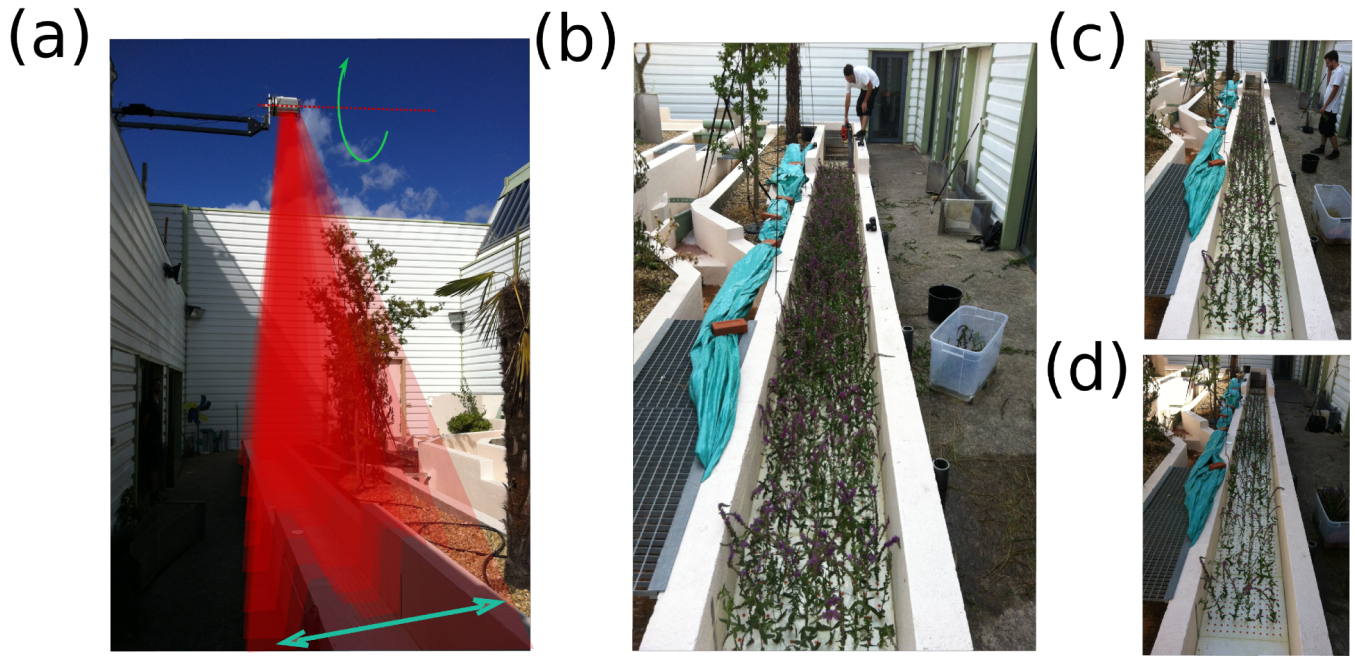

Figure 2: Illustration of the experimental setup. (a) the laser scanner and its scanning view (in red) through the channel flume. (b), (c), and (d) an example of species planting (*Lythrum salicaria*) at densities of 41, 82, 164 $plants.m^{-2}$, respectively.

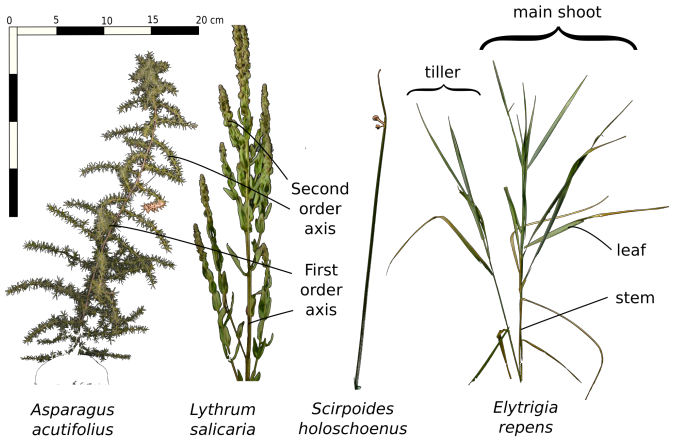

Figure 3: Illustration of the shape of selected species for the experiments.

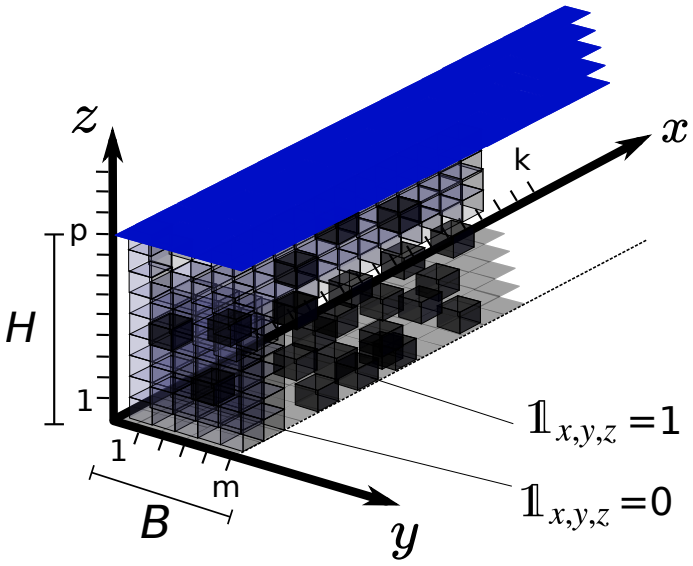

Figure 4: Illustration of point cloud voxelisation across the channel. H corresponds to the water level (in blue). Black and transparent voxels correspond to cubes that contained or not points issued from point cloud, respectively.

increments were both set to 0.04°, giving a scanning resolution of 7 mm at a distance of 10 m, corresponding to the range accuracy and precision of the scanner at this distance. TLS values were compared to manual measurements described in Table 1 only for vegetation height and FPA. The other variables cannot be accessed via the TLS clouds since cloud density was not high enough to identify a single plant architecture. Vegetation heights were directly issued from the cloud z-values, whereas FPA × planting density and FPA × number of plants rows along channel width were deduced from the computation of Bf_1 and Bf_2, respectively, as explained below.

We planted each combination of *plant* × *density* and we carried a first TLS scan. Then we opened the first sluice gate corresponding to a flow of 25.3 $L.s^{-}1$. After the steady flow was reached, measurements were taken, then we repeated the operation for the second flow corresponding to 51.4 $L.s^{-}1$.

2.6. Blockage factor estimates

TLS scans were first exported in referenced XYZ point clouds using Riscan Pro©software. Data clouds issued from the scans were scaled in the same local projection system to get length and width of the channel along X and Y-coordinates, respectively (see Figure 4 for definition of axes). Point clouds were first decimated using a mean nearest-neighbour distance filter and then voxelised using a voxelisation procedure illustrated in Figure 3 and similar to Jalonen et al. (2015)' approach. We defined a voxel resolution (here 1 mm^3) able to discriminate plant organs from TLS noise. Next $\mathbb{1}_{x,y,z}$ denotes the indicator function with 1 value when the TLS points are intercepted by the voxel, and 0 otherwise.

Then, we defined the density per voxel as $d_{y,z}$ by summing each voxels along X-axis and we divided by the total number of voxels along the channel length k to have a probability between 0 (no blockage) to 1 (complete blockage) (Equation 1) :

$$d_{y,z} = \frac{\sum_{x=1}^{k} \mathbb{1}_{x,y,z}}{k} \quad (1)$$

where,

- x, the position index of the voxel along the channel length
- y, the position index of the voxel along the channel width
- z, the position index of the voxel along the channel depth

We derived from the calculation of $d_{y,z}$ three possible definitions of the blockage factor Bf:

Bf_1 : the mean $d_{y,z}$ in a cross section (Equation 2). This blockage factor corresponds to the volume blockage factor as defined by Fisher (1992). Bf_1 is proportional to the FPA of each plant × planting density (Jalonen & Järvelä (2014)).

$$Bf_1 = \frac{\sum_{z=1}^{p} \sum_{y=1}^{m} d_{y,z}}{m \times p} \quad (2)$$

Bf_2 : the mean Bf_1 thresholded in selected and non selected pixels (Equation 3). The Bf_2 is similar to the frontal projected area of Jalonen & Järvelä (2014) over the whole channel. In other words, Bf_2 is proportional to the FPA of each plant × number of plants rows along y-axis.

$$Bf_2 = \mathbb{1}_{Bf_1 > s} \quad (3)$$

Bf_3 : the maximal height z of binarized $d_{x,z}$ according to the threshold s, summed over the channel width (Equation 4). Bf_3 is computed with all voxels beyond the canopy of the thresholded point cloud equal to 1. Bf_3 is thus computed from the mean canopy height model.

$$Bf_3 = \frac{\sum_{y=1}^{m} z_{max}(d_{y,z} > s)}{m \times p} \quad (4)$$

where,

- Bf_x, denotes a given Blockage factor metrics for point cloud.
- k, m, p denotes the number of voxels along x, y and z dimensions of the channel, respectively.
- s, denotes the threshold for $d_{y,z}$ binarization.

Here, the threshold value s was fixed to the $Q_{0.05}$ percentile of the $d_{y,z}$ distribution. According to the usual Wald confidence level on parameters, we chose to eliminate 5% of the lower extreme value of $d_{y,z}$ and considered the 5% percentile as the threshold for noise-free significant density.

2.7. Estimation of water flow resistance

Manning coefficients were estimated from the measured total head loss between upstream and downstream ends of the vegetated reach. To do so, we considered the backwater curve equation, expressed in its differential form:

$$\frac{dH}{dx} = \frac{S_b - S}{1 - F^2} \tag{5}$$

with

$$S = \frac{n^2 Q^2}{B^2 H^2 R^{4/3}} \tag{6}$$

in which S_b is the bed slope, S is the friction slope, n is the Manning parameter, Q is the discharge, B the canal width, R the hydraulic radius, H the water height, and F the Froude number. Equation 5 was solved by imposing the downstream boundary condition with the measured value at the downstream gauge, and the Runge-Kutta 4^{th} order approximation. Manning n was obtained by minimizing the error between calculated and observed backwater curve.

2.8. Relation between blockage factor and flow resistance

Based on non-linear nature of Manning-Blockage factors relationships (Green, 2005a), we linked the blocage factors Bf_x calculated to Manning coefficients using a simplified version of Nepf (2012) equation:

$$n = a \times (1 - Bf_x)^{-b} \times H^{(1/6)} \tag{7}$$

Non-linear Gauss-Newton fitting algorithm was used on Equation 7 to fit the a and b parameters.

3. Results

3.1. Blockage factor estimation at channel scale

Considering each species individually (Figure 5), sclerophyllous plants such as *Asparagus acutifolius* and *Lythrum salicaria* had the highest levels of $d_{y,z}$. Herbaceous plants such as *Elytrigia repens* presented a vertical heterogeneity due to the presence of several blades from each plant sucker laying on the ground, unlike to *Scirpoides holoschoenus* that exhibited a higher rigidity level. Despite presenting occlusions for the sclerophyllous species due to a single scan position, TLS point clouds gave consistent images of expected $d_{y,z}$ for each species. The threshold value s corresponding to d_y, z $Q_{0.05}$ percentile was 3.00e-4.

Blockage factor	Parameter	Estimate	Std. Error	t value	Pr(> |t|)
Bf1	a	0.06	0.01	8.93	0
(0 - 2e-04)	b	5492.28	693.77	7.9	0
Bf2	a	0.09	0.01	10.67	0
(0 - 0.24)	b	3.12	0.62	5.1	0
Bf3	a	0.08	0.00	18.14	0
(0 - 0.98)	b	0.27	0.02	13.5	0

Table 2: Table representing the values of a and b estimated from Non linear Gauss-Newton fitting algorithm on Equation 7. Values in brackets correspond to the range of each calculated blockage factor Bf.

Mean vegetation heights issued from TLS scans were underestimated by 5% compared to manual measurements of each singles plants. The range (min-max) of vegetation heights issued from TLS scans were similarly underestimated compared to manual measurements. Bf_1 and Bf_2 were correlated to FPA of each plant × plant density and FPA of each plant × number of plants rows along y-axis with a R^2=0.91 and 0.79, respectively (linear model, P-value<0.001, df=12). P-values of the intercepts of the linear models were both above 5%, indicating an absence of shift from TLS and manual measurements.

Video analysis from the three cameras revealed no reconfiguration of the plants, excepting the *Elytrigia repens* species that exhibited a blending of both main shoot and tillers of 10 ±2° and 40 ±10°, for first and second flow, respectively. This blending effect resulted in a deflected height reduction of 2% and 23%, respectively. We observed a small contraction of *Elytrigia repens* width with a bending of leaves toward flow direction, this qualitative observation being difficult to quantify regarding camera resolutions.

3.2. Estimation of water flow resistance

The calculated Manning coefficients were highly dependent on plant species, with the higher values of Manning for sclerophyllous species such as *Lythrum salicaria* and *Asparagus acutifolius* (Figure 6). The herbaceous plants *Scirpoides holoschoenus* and *Elytrigia repens* exhibited lower values of Manning. This may be explained partly by branching complexity which is higher in sclerophyllous species (Figure 3).

The relation between Manning and Bf_3 illustrated in Figure 6 was clearly non-linear and was in accordance with the simplified Equation 7. The non-linear relationship was also applied to the other calculated blockage factors. Plantation density was also positively correlated to Manning coefficient for all species, as shown in Figure 6. The error bars for n were obtained considering incertainties on level and discharge measurements.

3.3. Relation between blockage factor and flow resistance

Figure 7 showed that all Manning coefficients were well related to the blockage factors (R^2 ranging between 0.6-0.9, p-value < 0.05).

The models underestimated the highest values of n for Bf_1 and Bf_2, that corresponded to *Elytrigia repens* species.

All estimated parameters of Equation 7 were significant, with similar values for each calculated blockage factors, except for Bf_1, as denoted by Table 2. Value of parameter b was linked

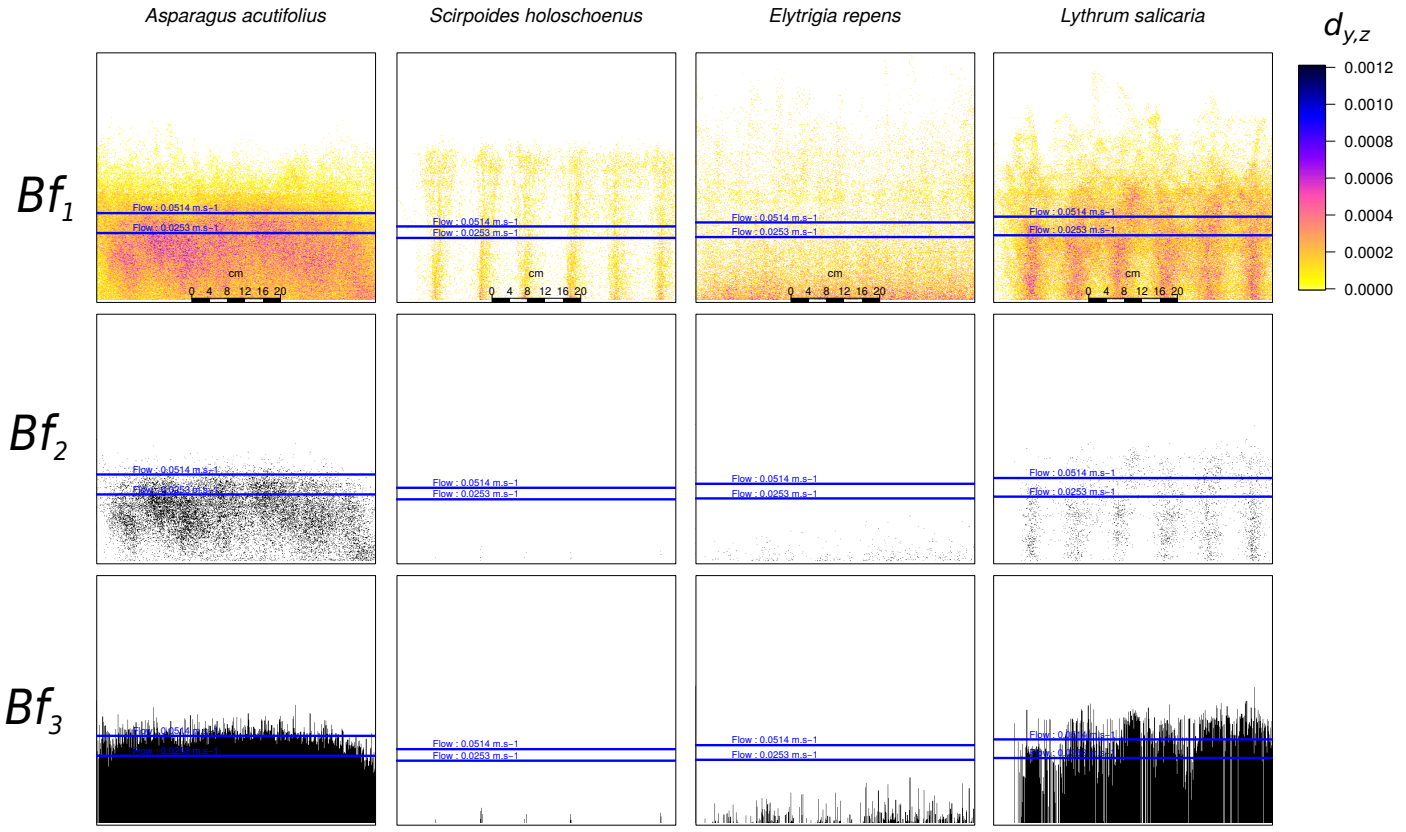

Figure 5: Description of calculated $d_{y,z}$ issued from point clouds voxelisation at 1 mm^3 resolution. We illustrated the results for each species planted at 82 $plants.m^{-2}$. Horizontal blue lines correspond to mean water level over the channel for the two different flows. First row corresponds to the illustration of Bf_1 by pixel colors. Second and third rows correspond to the illustrations of Bf_2 and Bf_3, respectively.

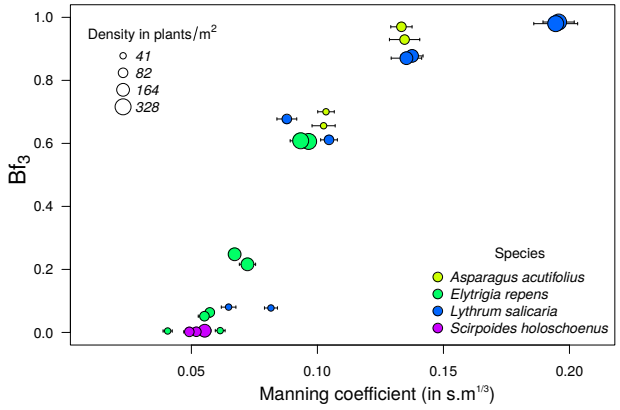

Figure 6: Relation between the calculated Manning (n) and calculated blockage factor Bf_3 for all species. Color and point size indicate a species and its density, respectively. Estimated errors issued from water depth variations were represented by horizontal segments.

to the range of each blockage factor calculated with the highest value for Bf_1.

4. Discussion and conclusions

Combining laser scanner and hydraulic flume in the same experiments helped disentangling the link between vegetation architecture and resistance factor. The different calculations of the blockage factor were best suited to the point clouds derived from the observations and could be used for further experimental studies using real vegetation material. We deduced from point cloud analysis that plant traits related to blockage factor were branching complexity and height. Jalonen & Järvelä (2014) highlighted the importance of stem and leaf areas for the estimation of drag forces. Weissteiner et al. (2015) concluded as well that branching complexity had a major effect on plant reconfiguration under hydrodynamic loading, figuring that this plant characteristic may affect greatly plant porosity against flow.

We explored a small part of plant diversity, but we could extrapolate our primary results to the whole diversity by using global database of plant traits (Kattge et al., 2011).

By focusing on vegetation of Mediterranean ditches, we explored a research avenue that differed from previous studies on rigid and homogoneous plant species (Nikora et al., 2008; Whittaker et al., 2013), aquatic macrophytes, shrubs or trees vegetation appearing in wide channels or rivers (Whittaker et al., 2013; Weissteiner et al., 2015). Herbaceous and sclerophyllous plants in Mediterranean ditches have smallest size, different biomechanical properties compared to macrophytes and shrubs. We followed work from Jalonen et al. (2015) on trees by using a voxelisation procedure of point clouds at a finer resolution (millimeter) to get consistent results for our small plants.

Considering laws relating blockage factors to Manning coefficients (Equation 7), our results are consistent with preliminary studies on the subject (Green, 2005b) with a a value of 0.07 derived from Luhar & Nepf (2013). The consistence of Equation 7 with observed data, taking into account the non-linear nature of the n-H and n-Bf_x relationships is in accordance with Green (2005b). The values of b, however, were substantially different from their estimated values 0.0239 given by (Luhar & Nepf, 2013). Bf_1 appears too small, which explains why b must be set very large in this case.

The best model relating Manning coefficients to blockage factor were issued from Equation 7 applied to Bf_3. It indicated that a measure of mean vegetation height could be sufficient to capture the resistance factor induced by vegetation cover, in accordance with results from Jalonen et al. (2015), provided that vegetation were uniformly distributed along the channel. The blockage factor Bf_1 that corresponds to the volume blockage factor of (Fisher, 1992) gave better results for the low Manning coefficients, i.e. $n < 0.1$, than Bf_2 and Bf_3, but failed to predict the high values of Manning. The thresold value s fixed at $Q_{0.05}$ percentile of the total distributions of d_y, z could explain that simulated Manning coefficients plateaued for values lower than 0.08.

The underestimation of Manning factors for herbaceous plants could be due to spatial plant reconfiguration against flow that limits friction factors (Whittaker et al., 2013; Poggi et al., 2009; Järvelä, 2005; Weissteiner et al., 2015). A further improvement of the blockage factor calculation should be to add a flexibility coefficient that reduced the potential blockage factor calculated without flow. This improvement could be adapted from observations in towing tanks from Weissteiner et al. (2015) on foliated trees, but with a reduced distance of underwater cameras from plants to get sufficient resolution level for deflection and contraction measures of plants.

Acknowledgments

Authors are grateful to the ONEMA and the INRA institutions who both funded the experimental work exposed in this paper within the 'Fossés Infiltrants et Pesticides' project (ONEMA) and the 'Pari-Scientifique: Hydro-écologie des fossés agricoles' project (INRA-EA). Authors thank also David Combemale and Dénes Király for their help in the channel flume. Authors are grateful for reviewer constructive comments that considerably ameliorated first manuscript draft.

The authors declare that there is no conflict of interest regarding the publication of this paper.

References

Benitou, K. (2013). Végétation de fond de canal et rugosité: Test d'un nouveau protocole expérimental. Technical report, AgroParisTech, Montpellier, France.

Boothroyd, R. J., Hardy, R. J., Warburton, J., & Marjoribanks, T. I. (2016). The importance of accurately representing submerged vegetation morphology in the numerical prediction of complex river flow. *Earth Surface Processes and Landforms*, *41*(4), 567–576.

Cassan, L., Belaud, G., Baume, J., & Dejean, C. (2015). Velocity profiles in a real vegetated channel. *Environmental Fluid Mechanics*, *15*(6), 1263–1279.

Champion, P. D. & Tanner, C. C. (2000). Seasonality of macrophytes and interaction with flow in a new zealand lowland stream. *Hydrobiologia*, *441*(1), 1–12.

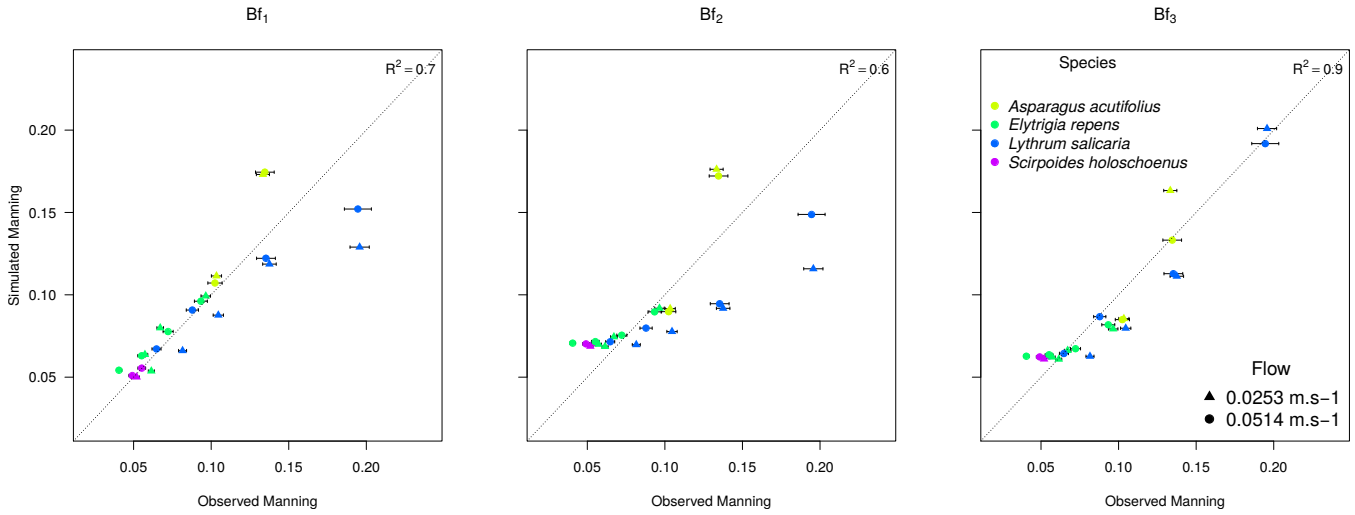

Figure 7: Comparison between observed Mannings and its simulated value using Equation 7 according to calculation of blockage factors from vegetation point clouds. Colors indicated the species, difference in flow values were symbolized by rounds and triangles. The dotted line corresponds to the perfect match between observations and simulations. Estimated errors issued from water depth variations were represented by horizontal segments.

Colbach, N., Collard, A., Guyot, S. H. M., Meziere, D., & Munier-Jolain, N. (2014). Assessing innovative sowing patterns for integrated weed management with a 3d crop:weed competition model. *European journal of agronomy*, *53*, 74–89.

Curran, J. C. & Hession, W. C. (2013). Vegetative impacts on hydraulics and sediment processes across the fluvial system. *Journal of Hydrology*, *505*, 364–376.

Dollinger, J., Dagès, C., Bailly, J.-S., Lagacherie, P., & Voltz, M. (2015). Managing ditches for agroecological engineering of landscape. A review. *Agronomy for Sustainable Development*, *35*(3), 999–1020.

Fisher, K. (1992). The hydraulic roughness of vegetated channels. *Report SR*, *305*.

Folkard, A. M. (2011). Vegetated flows in their environmental context: a review. *Proceedings of the ICE - Engineering and Computational Mechanics*, *164*(1), 3–24.

Godin, C. & Caraglio, Y. (1998). A Multiscale Model of Plant Topological Structures. *Journal of Theoretical Biology*, *191*(1), 1–46.

Green, J. C. (2005a). Comparison of blockage factors in modelling the resistance of channels containing submerged macrophytes. *River research and applications*, *21*(6), 671–686.

Green, J. C. (2005b). Modelling flow resistance in vegetated streams: review and development of new theory. *Hydrological processes*, *19*(6), 1245–1259.

Herzon, I. & Helenius, J. (2008). Agricultural drainage ditches, their biological importance and functioning. *Biological Conservation*, *141*(5), 1171–1183.

Jalonen, J. & Järvelä, J. (2014). Estimation of drag forces caused by natural woody vegetation of different scales. *Journal of Hydrodynamics, Ser. B*, *26*(4), 608–623.

Jalonen, J., Järvelä, J., & Aberle, J. (2012). Leaf area index as vegetation density measure for hydraulic analyses. *Journal of Hydraulic Engineering*, *139*(5), 461–469.

Jalonen, J., Järvelä, J., Koivusalo, H., & Hyyppä, H. (2014). Deriving floodplain topography and vegetation characteristics for hydraulic engineering applications by means of terrestrial laser scanning. *Journal of Hydraulic Engineering*, *140*(11), 1–12.

Jalonen, J., Järvelä, J., Virtanen, J.-P., Vaaja, M., Kurkela, M., & Hyyppä, H. (2015). Determining Characteristic Vegetation Areas by Terrestrial Laser Scanning for Floodplain Flow Modeling. *Water*, *7*(2), 420–437.

Järvelä, J. (2004). Determination of flow resistance caused by non [U+2010] submerged woody vegetation. *International Journal of River Basin Management*, *2*(1), 61–70.

Järvelä, J. (2005). Effect of submerged flexible vegetation on flow structure and resistance. *Journal of Hydrology*, *307*(1–4), 233–241.

Kattge, J., Díaz, S., Lavorel, S., Prentice, I. C., Leadley, P., Bönisch, G., Garnier, E., Westoby, M., Reich, P. B., Wright, I. J., Cornelissen, & al. (2011). TRY – a global database of plant traits. *Global Change Biology*, *17*(9), 2905–2935.

Kouwen, N., Unny, T., & Hill, H. M. (1969). Flow retardance in vegetated channels. *Journal of the Irrigation and Drainage Division*, *95*(2), 329–344.

Lepart, J. & Debussche, M. (1992). Human impact on landscape patterning: Mediterranean examples. In *Landscape boundaries* (pp. 76–106). Springer.

Levavasseur, F., Biarnès, A., Bailly, J., & Lagacherie, P. (2014). Time-varying impacts of different management regimes on vegetation cover in agricultural ditches. *Agricultural Water Management*, *140*(0), 14–19.

Luhar, M. & Nepf, H. M. (2013). From the blade scale to the reach scale: A characterization of aquatic vegetative drag. *Advances in Water Resources*, *51*, 305–316.

Marnotte, P. & Carrara, A. (2006). *Plantes des rizières de Camargue*. Montpellier, France: Editions Quae. Google-Books-ID: T_JvqEx7RP4C.

Nepf, H. M. (2012). Hydrodynamics of vegetated channels. *Journal of Hydraulic Research*, *50*(3), 262–279.

Nikora, V. (2010). Hydrodynamics of aquatic ecosystems: An interface between ecology, biomechanics and environmental fluid mechanics. *River Research and Applications*, *26*(4), 367–384.

Nikora, V., Larned, S., Nikora, N., Debnath, K., Cooper, G., & Reid, M. (2008). Hydraulic resistance due to aquatic vegetation in small streams: field study. *Journal of hydraulic engineering*, *134*(9), 1326–1332.

Nikuradse, J. (1933). *Strömungsgesetze in rauhen Rohren*. VDI-Verlag.

Pasquino, V., Gualtieri, P., & Doria, G. P. (2016). On evaluating flow resistance of rigid vegetation using classic hydraulic roughness at high submergence levels: An experimental work. In *Hydrodynamic and Mass Transport at Freshwater Aquatic Interfaces* (pp. 269–277). Springer.

Poggi, D., Krug, C., & Katul, G. G. (2009). Hydraulic resistance of submerged rigid vegetation derived from first-order closure models. *Water Resources Research*, *45*(10), 1–14.

Stephan, U. & Gutknecht, D. (2002). Hydraulic resistance of submerged flexible vegetation. *Journal of Hydrology*, *269*(1–2), 27–43.

Thomas, R. E., Johnson, M. F., Frostick, L. E., Parsons, D. R., Bouma, T. J., Dijkstra, J. T., Eiff, O., Gobert, S., Henry, P.-Y., Kemp, P., Mclelland, S. J., Moulin, F. Y., Myrhaug, D., Neyts, A., Paul, M., Penning, W. E., Puijalon, S., Rice, S. P., Stanica, A., Tagliapietra, D., Tal, M., Tørum, A., & Vousdoukas, M. I. (2014). Physical modelling of water, fauna and flora: knowledge gaps, avenues for future research and infrastructural needs. *Journal of Hydraulic Research*, *52*(3), 311–325.

Vargas-Luna, A., Crosato, A., & Uijttewaal, W. S. (2015). Effects of vegetation on flow and sediment transport: comparative analyses and validation of predicting models. *Earth Surface Processes and Landforms*, *40*(2), 157–176.

Watson, D. (1987). Hydraulic effects of aquatic weeds in uk rivers. *Regulated Rivers: Research & Management*, *1*(3), 211–227.

Weissteiner, C., Jalonen, J., Järvelä, J., & Rauch, H. P. (2015). Spatial–structural properties of woody riparian vegetation with a view to reconfiguration under hydrodynamic loading. *Ecological Engineering*, *85*, 85–94.

Whittaker, P., Wilson, C., Aberle, J., Rauch, H. P., & Xavier, P. (2013). A drag force model to incorporate the reconfiguration of full-scale riparian trees under hydrodynamic loading. *Journal of Hydraulic Research*, *51*(5), 569–580.

Wiens, J. A. (2002). Riverine landscapes: taking landscape ecology into the water. *Freshwater Biology*, *47*(4), 501–515.